Aerosol and Air Quality Research, 15: 2409–2421, 2015

ISSN: 1680-8584 print / 2071-1409 online
doi: 10.4209/aaqr.2015.03.0202

Pt Catalyst over SiO_2 and Al_2O_3 Supports Synthesized by Aerosol Method for HC-SCR DeNOx Application

Riyan Zahaf[1], Jae Wook Jung[1], Zachary Coker[2], Songkil Kim[3], Tae-Youl Choi[2], Donggeun Lee[1*]

[1] *School of Mechanical Engineering, Pusan Clean Coal Center, Pusan National University, Busan 609-735, Korea*
[2] *Department of Mechanical and Energy Engineering, University of North Texas, Denton, TX 76207, USA*
[3] *School of Mechanical Engineering, Georgia Institute of Technology, Atlanta, GA 30332, USA*

ABSTRACT

Silica-supported platinum (Pt/SiO_2) and alumina-supported platinum (Pt/Al_2O_3) catalysts have been prepared by an aerosol spray pyrolysis method. Systematic characterization of each catalyst using TEM, XRD, and XPS revealed that crystalline and metallic Pt nanoparticles were well dispersed on the surface of silica and alumina supports. The sintering effect on Pt particles over Al_2O_3 at high temperature (~250°C) is more prominent than those over SiO_2; this suggests that there is stronger interaction between Pt particles and SiO_2 support, when compared to Pt over Al_2O_3 support, resulting in Pt particles size below 3 nm. Moreover, steady-state catalytic experiments for selective reduction of nitrogen monoxide by propene have demonstrated that NO_x conversions to N_2O and N_2 in Pt/SiO_2 and Pt/Al_2O_3 catalysts are 29.8% and 55.8% at 250°C, respectively.

Keywords: Pt/SiO_2; Pt/Al_2O_3; Aerosol; DeNOx Catalyst.

INTRODUCTION

Emission of NO_x gases from both mobile and stationary sources causes serious environmental problems such as acid rain and photochemical smog (Pitchon and Fritz, 1999; Zhang *et al.*, 2011; Wanga *et al.*, 2012). Thus, NO_x treatment technologies have drawn much attention in view of catalysis, especially for treating various exhaust gases produced by state-of-the-art automobile engines (Haj *et al.*, 2002). Hydrocarbon (HC) species are often emitted from automobiles under lean-burn operating conditions, in the forms of fragments (propane, propene, etc.) and/or more primitive polycyclic aromatic hydrocarbons (PAHs) which are known as mutagenic and carcinogenic compounds causing cataracts, kidney, and liver damage (Lu *et al.*, 2011; Dong and Lee, 2009). Therefore, the European Union implemented increasingly stringent regulations on emissions, limiting HC and NO_x concentrations to lower than 0.17 g km^{-1} for passenger cars using diesel engines (The European Parliament and The Council of The European Union 2007).

The unburned HCs existing in the exhaust line can be used as a reducing agent for NO_x treatment (Pitchon and Fritz, 1999; Haj *et al.*, 2002) prior to tail-pipe emission, which is known as hydrocarbon-enhanced selective catalytic reduction (HC-SCR) of NO_x. Using the HCs for NO_x treatment enables more efficient fuel uses, while reducing HC and NO_x emissions under lean-burn conditions (Burch, 2004; Wang *et al.*, 2011). In this prospect, developing various catalysts for HC-SCR has been an intensive research area, which was initiated by Iwamoto *et al.* in 1990 (Iwamoto, 1990; Jayat *et al.*, 1999). Then, Burch (Burch and Millington, 1995; Burch and Millington, 1996; Burch and Watling, 1997; Burch and Watling, 1998; Burch *et al.*, 1998; Burch *et al.*, 2002; Burch, 2004) performed a series of pioneering investigations for revealing catalytic performance and reaction kinetics of HC-SCR catalysts. Among various formulations of catalysts including Ag, Pd, Co, Ni, Au, Rh, and Cu, Pt-based catalysts showed excellent performance for NO_x reduction at relatively low temperatures (Burch and Millington, 1995, 1996; Burch and Watling, 1997; Jayat *et al.*, 1999; Burch *et al.*, 2002). However, platinum suffers from three serious drawbacks: a narrow temperature window of operation, an objectionably high selectivity toward N_2O (Burch and Watling, 1997) rather than a major species of NO or NO_2, and a poor thermal stability (Asoro *et al.*, 2010). In an attempt to resolve the issue of thermal stability, namely that Pt particles are easily sintered into large sizes, thereby significantly changing their behavior and catalytic performance (Suzuki *et al.*, 2010), supporting materials such as silica and alumina have been introduced (Gonzalez *et al.*, 1997; Nagai *et al.*, 2006). As an example, Burch *et al.* (1996) reported that the maximum conversion of NO for Pt/SiO_2 and Pt/Al_2O_3

* Corresponding author.
Tel.: +82-51-510-2365; Fax: +82-51-512-5236
E-mail address: donglee@pusan.ac.kr

catalysts reached 75% and 60%, respectively. Furthermore, such metal oxide supports are known to lower the working temperatures of Pt catalysts and minimize the undesirable corrosion effect of water vapor and sulfur oxides (SO_x) (Burch and Watling, 1997; Gonzalez *et al.*, 1997; Männikkö *et al.*, 2012).

Recent studies suggested that specific catalytic activities are sensitive to not only the reducing gases and supporting materials, but also the dispersion, size, crystallographic nature, and microstructure of the Pt catalysts (Seker and Gulari, 2000; García-Cortés *et al.*, 2003; Vaccaro *et al.*, 2003; Després *et al.*, 2004; Radic *et al.*, 2004; Mulla *et al.*, 2006). Given a limited amount of precious Pt in a sample, well-dispersed Pt particles with a moderate size (3–7 nm) are ideal for efficient conversion of NO_x (Jayat *et al.*, 1999; Vaccaro *et al.*, 2003; García-Cortés *et al.*, 2003; Després *et al.*, 2004). The existence of very large particles (> 10 nm) can cause a significant deterioration in particle dispersion, and can lead to less catalytic activity. Very small particles (< 2 nm) result in far better dispersion, but easy oxidation, which causes deactivation of the catalytic function (García-Cortés *et al.*, 2003). In addition, crystallographic orientation of Pt determined by the ratio of Pt (100) peak to Pt (111) peak from X-ray diffraction may affect N_2 selectivity because NO molecules can be dissociatively adsorbed on Pt (100), while NO is mostly adsorbed molecularly on Pt (110) and Pt (111) (García-Cortés *et al.*, 2003). Regarding the chemical oxidation state of Pt, several researchers (Després *et al.*, 2004; Mulla *et al.*, 2006) reported that formation of PtO and PtO_2 can degrade catalytic activity and eventually lead to deactivation of the catalyst. Another important factor determining catalytic activity is the catalyst preparation method; some materials prepared by the sol-gel method show improved activity and N_2 selectivity, even in the presence of high water vapor concentrations (2.6–10%) (Seker and Gulari, 2000; Burch *et al.*, 2002).

The Pt catalysts on metal oxide supports produced by the incipient wetness impregnation and ion-exchange methods (Burch and Millington, 1995, 1996; Burch and Watling, 1997; Burch *et al.*, 1998; Männikkö *et al.*, 2012) have been used to reveal that the aforementioned thermal stability problem is due to weak interactions with Pt and the supporting material. It has been established that the thermal stability issue with Pt is less severe in catalysts synthesized by the sol-gel method (Gonzalez *et al.*, 1997; Cho *et al.*, 1998; Romero-Pascual *et al.*, 2002; Hu *et al.*, 2006). Alternatively, flame spray pyrolysis (FSP) has been used for producing alumina-supported platinum catalysts (Strobel *et al.*, 2003, 2006). More recently, the aerosol-based process has been widely investigated and used for making catalysts for deNOx (Boningari *et al.*, 2012), deVOCs (Lin *et al.*, 2015), deCO (Byeon *et al.*, 2014) applications. While the aerosol methods have been recognized to be well developed, the methods have had limited success in control of agglomeration of catalysts. The uncontrolled agglomeration might reduce exposed surface areas of catalysts, leading to degradation of catalytic activity and performance.

Thus, we focused on the agglomeration/microstructural control and thermal stability of catalysts. Combining the sol-gel method with the aerosol spray-pyrolysis method (called the aerosol-gel method hereafter), we may take the unique benefits of each method (Lee *et al.*, 2007; Firmansyah *et al.*, 2009, 2012), together with the advantage of cost-effective production of microstructure-controlled particles (Lee *et al.*, 1997; Santiago *et al.*, 2011). Better understanding the process, one can extend this method to the synthesis of binary hetero-structured catalysts.

In this study, we have applied the aerosol method for the synthesis of well-dispersed Pt particles on SiO_2 and Al_2O_3 supports The two types of catalysts exhibited comparable NO conversion with respect to the previous reports. The effect of sintering on particle size distribution and relevant possible mechanisms were explored.

EXPERIMENTAL METHODS

Preparation of Catalysts

A precursor solution for Pt/SiO_2 catalysts was prepared as follows: 56 mg platinum (II) acetylacetonate ($Pt(acac)_2$, Aldrich, 97%) well dissolved in 33.6 mL ethanol (Aldrich, 99.5%), was mixed with 3.2 mL TEOS (Aldrich, 98%) dissolved in 17.6 mL ethanol (Aldrich, 99.5%), and the mixture solution was stirred at room temperature for 30 min. Then, 12.5 mL deionized (DI) water and 1.2 mL HCl (0.1 M) were introduced to the mixture, and then the solution was stirred at room temperature for 2 hours in order to initiate the sol-gel reaction of TEOS with water. Herein only SiO_2 sols are formed, maintaining the $Pt(acac)_2$ dissolved in the solution at low temperature.

A precursor solution for Pt/Al_2O_3 catalysts was prepared likewise: 40 mg $Pt(acac)_2$ was first dissolved in 40 mL ethanol and stirred at 50°C for 30 minutes. A second solution was made by dissolving 800 mg aluminum nitrate nonahydrate (ANN, Aldrich, 98%) into 40 ml ethanol. The two solutions were mixed together, and stirred at 50°C for 30 minutes. Then, 20 mL of water and 0.1 mL of HCl (0.1 M) were introduced into the solution and stirred again under 50°C for two days.

As-prepared two different solutions were aerosolized to 1–5 μm droplets in an atomizer running with compressed air at a pressure of 25 psi and a gas flow rate of 2.2 L min^{-1}. The droplets were therefore fed into a diffusion dryer, filled with silica gel to remove the solvent. They were then transferred to a quartz tube (1/4" in diameter), and heated by tube furnace, in which $Pt(acac)_2$ is pyrolyzed to form tiny Pt nanoparticles. It should be noted that the droplets contain not only SiO_2 sols and Pt aggregates but also remaining TEOS solution and $Pt(acac)_2$, in the case of Pt/SiO_2 catalysts. In the case of Pt/Al_2O_3, however, the droplets contain liquid-phase reactants of $Pt(acac)_2$ and $Al(NO_3)_3$ until the reactant temperatures reach an adequate level in the furnace; this occurs as aluminum nitrate is never sol-gel reacted, but rather pyrolyzed at high temperature. It is noted that organic species in TEOS and $Pt(acac)_2$ appear to leave carbon behind after the decomposition reaction when Ar was used instead of air. This is the reason why air has been used as a carrier gas.

The formation positions of solid particles (i.e., Pt with respect to its metal oxide support) can vary depending on

the differences in their reaction kinetics. The disparity in formation timing of Pt and metal oxides enables control of the morphology in such a way that Pt dots are formed on the outer surface of the SiO_2 or Al_2O_3 particles. For reference (control) materials, pure SiO_2 or Al_2O_3 nanoparticles were also prepared in the same way as described above (without Pt source), and then examined for their performance as catalytic promoters. The residence time of particles in the furnace is estimated at approximately 0.19 s. The reacting temperature of the furnace was set to either 600°C for Pt/SiO_2 catalysts, or 700°C for Pt/Al_2O_3 catalysts. As-synthesized catalysts nanoparticles were collected by a glass membrane filter with 1 μm pores (Milipore). More details about experimental setup are available elsewhere (Lee *et al.*, 2007; Firmansyah *et al.*, 2009, 2012).

Characterization of Catalysts

As-prepared catalysts particles were dispersed in ethanol with an ultrasonicator. A few milliliters of the suspension were dropped onto a carbon-coated TEM grid and then dried in air. The size and morphology of the catalysts were observed by a high-resolution transmission electron microscope (HR-TEM; JEM 2010F & 2011, JEOL, 200 kV) equipped with an energy dispersive spectrometer (EDS). Crystalline phase of the samples was characterized in view of mole composition and crystallite size by using X-ray photoelectron spectroscopy (XPS; ESCALAB 250 XPS spectrometer) with Al Kα X-ray (1486.6 eV) with a resolution of 0.45 eV and X-ray diffraction (Bruker, AXS) with Cu Kα radiation (λ = 0.154 nm), respectively. Pt loading was measured by an inductive coupled plasma optical emission spectrometer (ICP-OES; JY ULTIMA 2 C HR, Horiba).

Test for Catalytic Activity of NO Reduction

Catalytic performance of each sample was tested as follows: each powder sample weighing 34 mg was placed inside a 1/8" diameter tube with 1 cm length, where both tube ends were blocked by a layer of glass wool. The tube was connected to 1/4" stainless steel tubes in a way that the sample holder was located at the center of a tube furnace, and provided, a reactant gas mixture composed of 236 ppm NO, 440 ppm C_3H_6, and 5% O_2 in He. Before testing, the powder samples were heated to temperatures up to 700°C for 4 minutes, with sufficient air flow to flush out any remaining liquid solvent from the sample. The samples were then cooled under Ar flow to 150°C. The temperature of the sample holder was controlled to a designated temperature in a range of 150–400°C. After the desired temperature was reached, the reactant gases began to flow through the catalyst bed in the sample holder at a total flow rate of 66 ccm. The mole composition of the reactant gases before and after passing through the catalyst bed was measured with Fourier transform infrared spectroscopy (FTIR; Nicolet 380, Thermo Electron) equipped with a 10-m optical-path gas cell.

The FTIR measurement was performed over a range of 800–2800 cm^{-1} with a resolution of 4 cm^{-1}. A calibration experiment was performed to obtain a correlation between the known composition and the resultant peak intensity for gases including NO, C_3H_6, CO_2, N_2O, and NO_2 at steady state. The resultant conversion efficiency (C_Z) of gas species Z, e.g., NO or C_3H_6 gases, was calculated as follows:

$$C_{NO} = \frac{[NO]_I - [NO]_T}{[NO]_I} \times 100 \quad (1)$$

$$C_{C3H6} = \frac{[C_3H_6]_I - [C_3H_6]_T}{[C_3H_6]_I} \times 100, \quad (2)$$

where $[Z]_I$ and $[Z]_T$ are the concentrations of the gas, Z, which were measured before and after the sample holder, respectively. There was no measured NO_2 species in the inlet for all temperatures (before sample holder), however, NO_2 species was generated immediately upon the contact of NO gas with Pt catalysts at temperatures higher than 250°C, causing full propene conversion (García-Cortés *et al.*, 2003). The relative yield, X_Z, and selectivity, S_Z, of a product Z are defined as follows (Joubert *et al.*, 2006):

$$X_Z = \frac{n([Z]_I - [Z]_T)}{[NOx]_I} \times 100 \quad (3)$$

$$S_Z = \frac{n([Z]_I - [Z]_T)}{[NOx]_I - [NOx]_T} \times 100, \quad (4)$$

where n is the number of nitrogen atoms in the gas Z. The N-containing products (Z) of the reaction are N_2, N_2O, and NO_2. N_2 cannot be detected by FTIR; therefore the product yield of N_2 is given by (Pitchon and Fritz 1999):

$$X_{N_2} = C_{NO} - X_{N_2O} - X_{NO_2} = C_{NOx} - X_{N_2O} \quad (5)$$

RESULTS AND DISCUSSION

Fig. 1(a) shows a typical TEM image of the as-prepared Pt/SiO_2 catalysts produced by the aerosol method. During the time for sol-gel reaction in the atomizer (2 hours in this study), small silica sols and aggregates were suspended in a colloidal solution, in which $Pt(acac)_2$ and a part of TEOS remain dissolved. The solution was aerosolized, subsequently heated up, and finally turned into spherical nanoparticles. Through HR-TEM characterization, it was revealed that the many tiny dark dots covering the large gray spheres were in-fact metallic Pt dots on the surface of amorphous silica spheres. Unlike the case of Pt/SiO_2, with Pt/Al_2O_3, two precursors of $Pt(acac)_2$ and $Al(NO_3)_3$ remain dissolved in the atomized droplets, until they are decomposed to solid phase at high temperatures. Nevertheless, Fig. 1(b) shows a very similar HR-TEM image of Pt/Al_2O_3 catalysts: Pt dots on large Al_2O_3 spheres. The sizes of Pt in both cases were measured and their size distributions from TEM image analysis are displayed in Fig. 1(c): more than 350 Pt nanoparticles in each case were considered and the same set of Pt particles were measured twice to yield an average diameter in an attempt to reduce the uncertainty for size

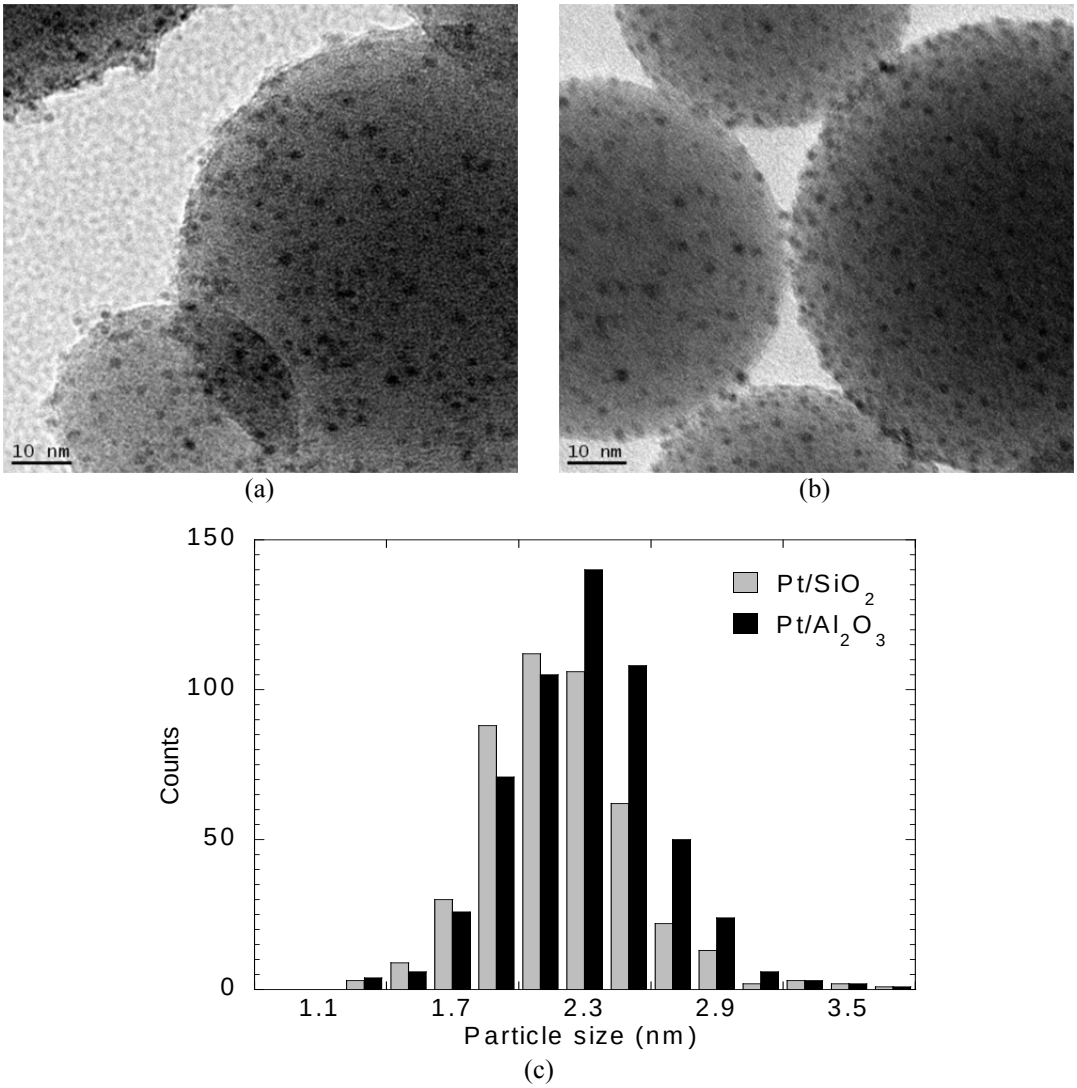

Fig. 1. a) TEM micrograph of Pt/SiO_2, b) TEM micrograph of Pt/Al_2O_3, c) Histogram plot of particle size distribution for Pt/SiO_2 and Pt/Al_2O_3 catalyst. The Pt particles are indicated by the black dot on the surface of larger spherical particles.

measurement of the catalysts. As a result, the Pt dots are distributed from 1.3 to 3.5 nm in diameter, with mode diameters of 1.9 and 2.3 nm for Pt/SiO_2 and Pt/Al_2O_3, respectively. The larger size of Pt dots when supported by Al_2O_3 is likely attributed to higher furnace temperature, which might facilitate to sinter Pt particles into larger dots. Additionally, it can be postulated that, in the absence of sol-gel reactions which can form a matrix structure to anchor the Pt particles (Firmansyah *et al.*, 2012), coproduced Pt dots may have a better chance to move and sinter on the surface of alumina spheres.

Of particular interest is understanding the formation mechanism of Pt dots on the surface of the metal oxide spheres, in view of size and hetero-structure of Pt particles; when a droplet evaporates during the spray-pyrolysis process, the dissolved solutes are locally concentrated near the droplet surface, and diffuse toward the center of the droplet in response to the concentration gradient, while the solvent diffuses toward the outermost region, and evaporates. It is generally accepted that the overall morphology of single-component particles is determined by the competition of solute diffusion and solvent evaporation rates (Jayanthi *et al.*, 1993; Lenggoro *et al.*, 2000; Lee *et al.*, 2007). In the present study, there are two diffusing solutes in a solvent droplet: for Pt/SiO_2 there are non-ionic molecules of $Pt(acac)_2$ and TEOS, and for Pt/Al_2O_3, there are $Pt(acac)_2$ molecules and Al^{3+} ions (from dissolved ANN). A disparity of relative diffusion speed between the solutes likely determines local abundances of the solutes, in a way that a fast diffusing solute moves toward the droplet center more quickly than a slowly diffusing solute. Noting that product particles come out of the abundant regions, the existence of Pt dots on the surface seems to indicate that the solute of $Pt(acac)_2$ is the least diffusing species. In order to confirm that the diffusion coefficients of the three solute species, as a measure of the diffusion rate, are estimated to compare as follows.

The diffusion coefficient of Al^{3+} ion in a dilute solution at 298 K was determined according to Nernst-Haskell equation: $D_s = 298R_g\,(1/v^+ + 1/v^-)/F^2(1/\lambda^0_+ + 1/\lambda^0_-)$, where R_g is the gas constant, F is the Faraday constant, v^+ and v^-

are respectively the valences of the cation and anion, and λ^0 is the limiting ionic conductance (Reid *et al.*, 1987; Firmansyah *et al.*, 2009, 2012). In this study, the D_s value for Al^{3+} ions is estimated to be 1.15×10^{-5} cm^2 s^{-1} via $v^{Al3+} = 3$, $v^{NO3-} = 1$, $\lambda^0_{Al3+} = 59.0$ Ω^{-1} cm^2 mol^{-1} and $\lambda^0_{NO3-} = 71.4$ Ω^{-1} cm^2 mol^{-1}. For nonionic solutes of TEOS and Pt(acac)$_2$, the corresponding values of D_s are calculated by Wilke and Chang's equation (Reid *et al.*, 1987; Firmansyah *et al.*, 2009, 2012): $D_s^0 = 7.4 \times 10^{-8}(\phi M_B)^{1/2} T[\eta_B V_A^{0.6}]$, where M_B is the solvent molecular weight in g mol^{-1}, η_B is the solvent viscosity in cP, V_A is the molar volume of solute A at its normal boiling temperature in cm^3 mol^{-1}, and ϕ is the association factor. As a result, the diffusion coefficient of Pt(acac)$_2$ in ethanol is estimated to be 4.1×10^{-6} cm^2 s^{-1} and the diffusion coefficient of TEOS in water is estimated at 8.0×10^{-6} cm^2 s^{-1}. It is quite clear that the lighter species of TEOS and Al^{3+} diffuse to the droplet center at higher speeds, leaving behind the heaviest Pt(acac)$_2$ near the surface; this may explain why Pt(acac)$_2$ decomposes to Pt dots mainly on the surface of the silica and alumina spheres. Another route to explain the presence of Pt on the surface of the metal oxide supports is from a disparity of evaporation rates between water and ethanol. It is noted that Pt(acac)$_2$ dissolves mainly in ethanol which is 40% more volatile than water (Reid *et al.*, 1987), while TEOS and Al^{3+} dissolves in water. Hence, faster evaporation/consumption of ethanol near a droplet surface initiates the precipitation of Pt(acac)$_2$ whereas TEOS and $Al(NO_3)_3$ both retreat to the center along with shrinking water. This is likely how a pair of solutes is segregated.

Figs. 2(a) and 2(b) show XRD patterns of Pt/SiO_2 and Pt/Al_2O_3 catalysts in comparison with those of SiO_2 and Al_2O_3 supports only, respectively. Fig. 2(a) clearly shows four major peaks of (111), (200), (220), and (331) crystalline facets of Pt as well as a very broad peak at ~23° in 2θ units. The broad peak also appears in the pure SiO_2 sample, indicating that the silica is almost amorphous. Likewise, Fig. 2(b) shows similar diffraction patterns of crystalline Pt on a mixture of amorphous and γ-phase alumina. Scherrer equation (Wang *et al.*, 2006) is applied to the largest peak of Pt (111) so that the crystallite size for Pt/SiO_2 and Pt/Al_2O_3 are estimated as 2.8 nm and 3.1 nm, respectively, which is consistent with TEM image analysis as shown in Fig. 1(c).

The oxidation states of Pt on silica and alumina supports are examined by XPS. Fig. 3(a) shows that the Pt 4f core-level XPS spectrum of Pt/SiO_2 catalysts is mainly composed of three pairs of doublets. The highest doublet (at 71.2 and 74.7 eV) corresponds to metallic Pt. The second highest doublet (at 72.3 and 75.5 eV), 1 eV blue-shifted from the

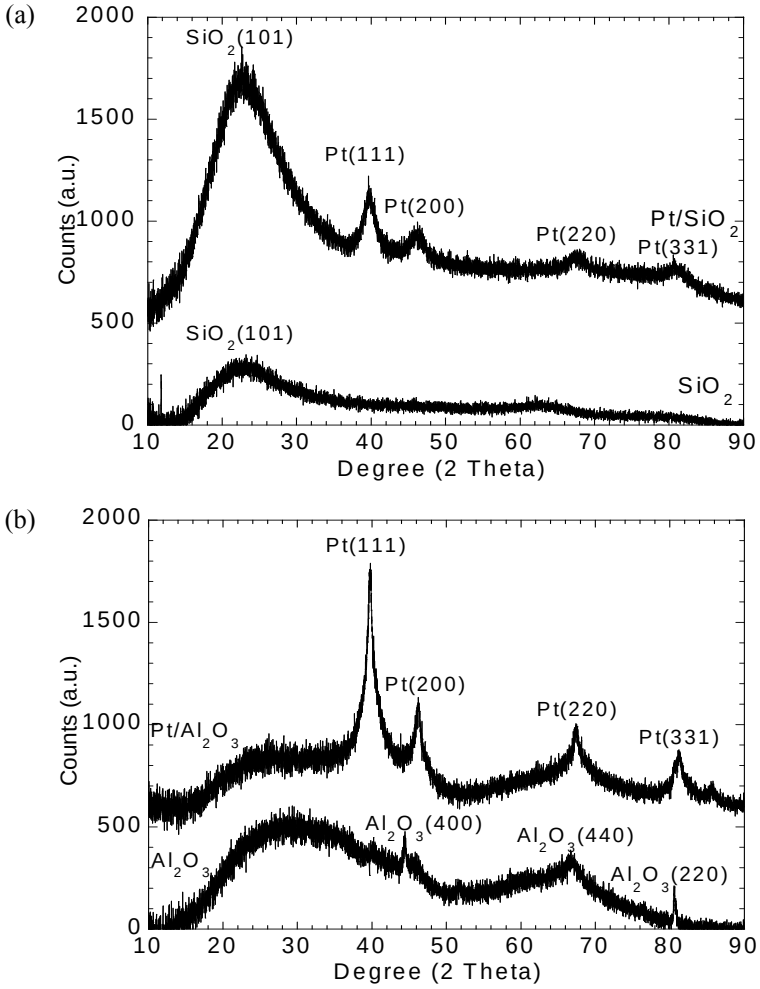

Fig. 2. XRD pattern for: a) Pt/SiO_2, b) Pt/Al_2O_3.

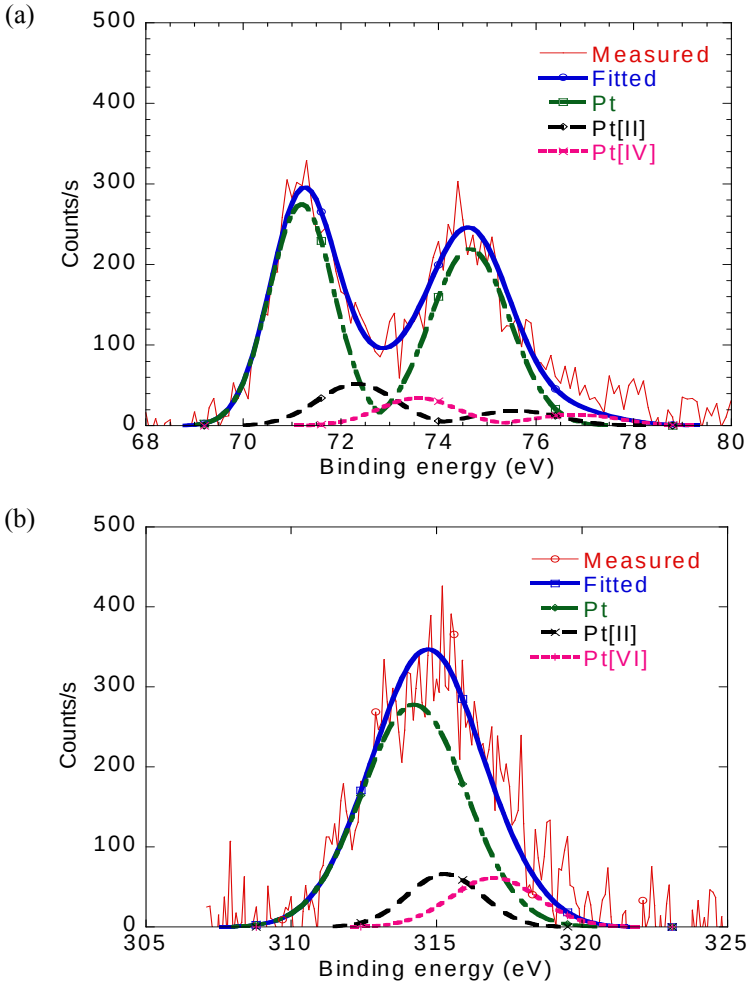

Fig. 3. Photoelectron spectra and peak decomposition for: a) Pt 4f of Pt/SiO_2, b) Pt 4f of Pt/Al_2O_3, c) Pt 4d of Pt/Al_2O_3.

metallic peaks of Pt, is assigned to Pt [II] states as in PtO or $Pt(OH)_2$. The weakest third doublet at 73.6 and 76.7 eV suggests that a minor level of Pt [IV] as in PtO_2 exists in the present catalysts (Kang *et al.*, 2005; Choi *et al.*, 2010). For Pt/Al_2O_3 catalysts, however, the Pt 4f core-level XPS spectrum is considerably different from that of Pt/SiO_2, mainly because the Pt 4f lines are overlapped with the Al 2p lines. Because of this interference, it is almost impossible to measure the $4f_{5/2}$ peak intensity of Pt on alumina especially when the Pt content is below 5%. Hence, the Pt $4d_{5/2}$ line is measured as an alternative (Shyu and Otto, 1988). Fig. 3(b) shows the Pt $4d_{5/2}$ core-level XPS spectrum of Pt/Al_2O_3 catalysts deconvoluted to three subpeaks. In Fig. 3(b), the highest peak at 314 eV is the signal from metallic Pt (Shyu and Otto 1988). The second peak at 315.3 eV is assigned to Pt [II] state as in PtO or $Pt(OH)_2$ (Shyu and Otto, 1988). The third peak at 316.9 eV corresponds to Pt [IV], indicating the existence of PtO_2 (Shyu and Otto, 1988). The surface-oxygenated species of PtO and PtO_2 in the as-prepared Pt catalysts, which are presumably produced during the decomposition reaction at elevated temperatures of 600°C (for Pt/SiO_2) and 700°C (for Pt/Al_2O_3) in air (Hauff *et al.*, 2012), are believed to hinder the NOx dissociation on the surface of metallic Pt (Romero-Pascual *et al.*, 2002; Hu *et al.*, 2006). Considering that the relative abundance of Pt, PtO, and PtO_2 is often approximated by the corresponding XPS peak area, one may notice from Figs. 3(a) and 3(b) that metallic Pt, as a major species, dominates other minor species of PtO and PtO_2. Furthermore, relative abundance of each species approximated from the surface area of deconvoluted peaks in Figs. 3(a) and 3(b), and shown in Table 1, indicates that metallic Pt^0 is dominant for both catalysts. The value of metallic Pt^0 reported here (73%–78%) are in good agreement with previous results for the Pt samples heat treated by flowing H_2/N_2 at 450°C (Despres *et al.*, 2004) or N_2 at 1500°C (Kang *et al.*, 2005).

The overall HC-SCR reaction for the produced catalysts of Pt/SiO_2 or Pt/Al_2O_3 is described as:

$$a\mathrm{NO} + b\mathrm{C_3H_6} + c\mathrm{O_2} \rightarrow d\mathrm{N_2} + e\mathrm{NO_2} + f\mathrm{N_2O} + g\mathrm{H_2O} + h\mathrm{CO_2}, \quad (6)$$

where the coefficients of *a*, *b*, *c*, *d*, *e*, *f*, *g*, and *h* are dependent on the types of catalysts, reactant concentration, and temperature. To investigate the reaction mechanism, a compositional analysis for the mixture of the reactants and the products was performed using gas-cell FTIR. Figs. 4(a)–4(d) show FTIR spectra obtained before and after

Table 1. The relative abundance of different Pt species determined from Peak Deconvolution of XPS measurements.

Sample	% Area of relative abundance		
	Pt	PtO	PtO_2
Pt/SiO_2	78.5	12.7	8.72
Pt/Al_2O_3	73.5	12.6	13.7

passing the reactant gases in Eq. (7) through SiO_2, Al_2O_3, Pt/SiO_2 and Pt/Al_2O_3 catalysts tested at different temperatures, respectively. FTIR spectrum at the bottom of each figure indicates a little but distinct peak of CO_2 even before contacting the catalysts. The trace level of CO_2 is believed to come from indoor atmosphere by gaseous diffusion to the gas cell of the FTIR machine. Two small double peaks at 1820–1960 cm^{-1} are assigned to NO gas (Smith *et al.*, 1988) and marked with a dotted box. Other peaks at 912 cm^{-1}, 1598 cm^{-1} and 2210 cm^{-1} are assigned to C_3H_6 (Yoon *et al.*, 2002), NO_2 (Li and Guan, 2009) and N_2O (Sobczak *et al.*, 2008), respectively. Though the peak of NO_2 gas is overlapped with that of H_2O (Tshilongo *et al.*, 2009) at ~1600 cm^{-1}, it is quite clear at which temperature the NO_2 gas peak begins to be prominent in the presence of Pt (see Figs. 4(c) and 4(d)).

Figs. 4(a) and 4(b) show the spectrum of evolved gases from the catalytic support of SiO_2 and Al_2O_3 without Pt. The profiles of spectrum for 150°C and 200°C are almost the same as the inlet, implying that there is no catalytic activity of the supports in this temperature range. At temperatures of 250°C and 300°C, we observe propene combustion catalyzed by metal oxide support in which the SiO_2 support appears more active than that of Al_2O_3; this is due to the fact that NOx and O_2 cannot form an adsorbed species on the inert support of SiO_2. As a result, O_2(g) will react directly with hydrocarbon in the gas phase to generate CO_2 and H_2O when the temperature is higher than 250°C. On the other hand, NO_x and O_2 can form an adsorbed species (NO_{ads}) (Burch *et al.*, 1998) on Al_2O_3 which has higher surface acidity (Hirashima *et al.*, 1998). In this case, hydrocarbon loses chance to react with O_2(g) in the gas phase, rather reacts with NO_{ads} at higher temperatures, and eventually generate CO_2 and H_2O. For this reason, alumina might be apparently less active than

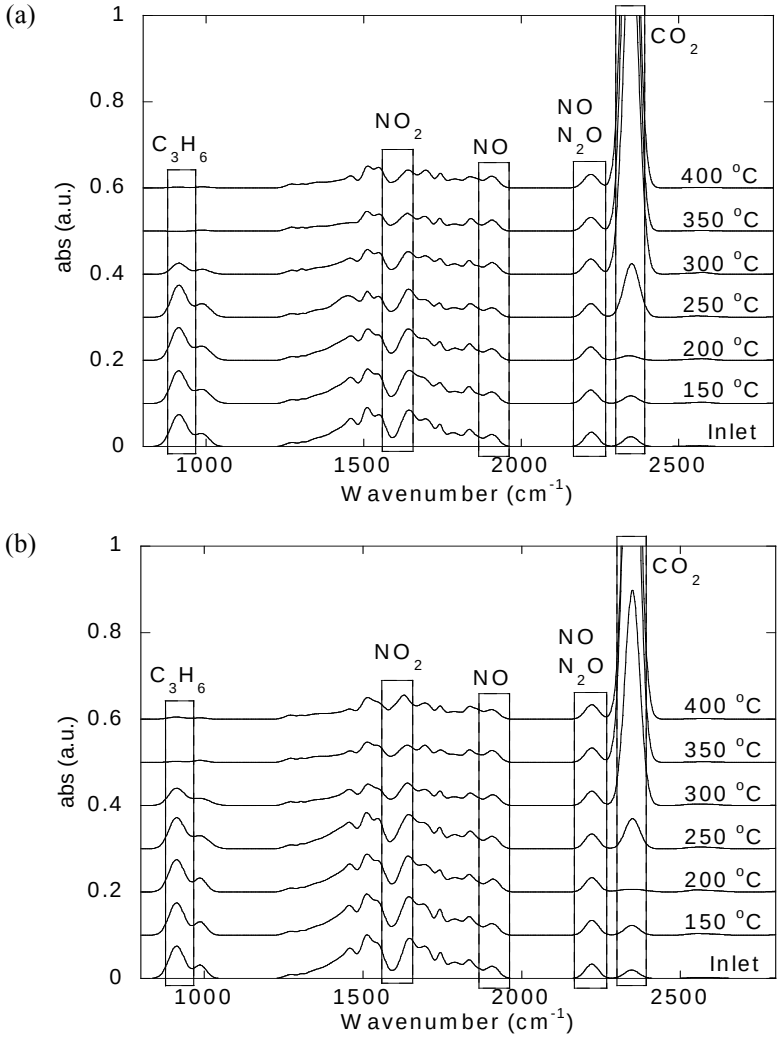

Fig. 4. Gas FTIR spectra with the increasing temperature for samples: a) SiO_2 only, b) Al_2O_3 only, c) Pt/SiO_2, and d) Pt/Al_2O_3.

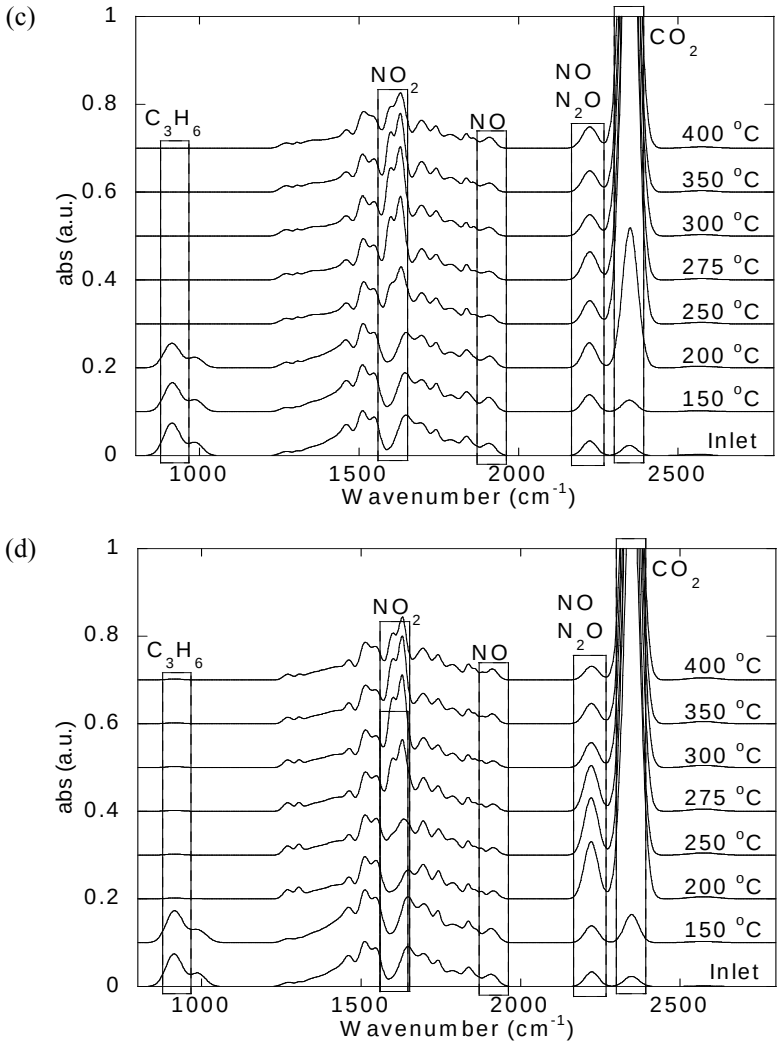

Fig. 4. (*continued*).

silica for hydrocarbon oxidation. At temperatures of 350°C and 400°C, NO reduction of about 20% is observed with Al_2O_3 catalysts, while NO reduction with SiO_2 is not observed at any temperatures tested. These facts suggest that Al_2O_3 should be more favorable as a catalyst support for the NO treatment than SiO_2, and may contribute to better activity when it is combined with Pt.

For Pt/SiO_2 catalyst at 150°C, the spectrum is almost identical to that of original reactant gas mixtures (noted as 'inlet' in Fig. 4(c)). As temperature is increased to 200°C, the peaks of NO and C_3H_6 exhibit a slight decrease, while the peaks of N_2O and CO_2 species show distinctive increases. This suggests that NO gas is partly reduced to N_2O and N_2, and that the O from the catalyst surface might be consumed to oxidize the incoming C_3H_6 gas to generate CO_2. This is exactly how HC-SCR catalysts are supposed to function via a redox process (Burch and Millington, 1996). A dramatic change is observed in every gas species when the temperature is increased further to 250°C: a sudden disappearance of C_3H_6, associated with a huge increase in CO_2 peak, a relatively large decrease in NO peak height, a noticeable increase of NO_2 peak, and a sudden stop to change in N_2O peak. Unlike the first three observations, the fourth and fifth observations indicate that NO is not properly reduced to N_2O or N_2, but rather oxidized to NO_2 even at the expense of C_3H_6. The preferential oxidation of NO suggests that there is more abundant chemisorbed oxygen than chemisorbed nitrogen on Pt, making the oxidation more probable than reduction. A larger peak of NO_2 and a small peak of N_2O at 275°C and at 300°C were observed; the conversion of NO to NO_2 for Pt/SiO_2 at these temperatures is similar with the catalytic result as reported by Jayat *et al.* (1999). Moreover, the role of C_3H_6 in consuming the chemisorbed oxygen at the Pt surface becomes insignificant as the catalyst surface is almost completely covered by chemisorbed oxygen. As the temperature is increased to 350°C, the NO_2 peak and NO peaks slightly decrease, starting at this temperature, generation of gas phase NO_2 from the catalyst is limited by the NO_2 equilibrium concentration as indicated by previous authors (Seker and Gulari, 2000; García-Cortés *et al.*, 2003). Eventually, when the temperature is increased to 400°C, C_3H_6 and N_2O almost completely disappear, suggesting that Pt oxidation is predominantly arising, which eventually leads to the degradation process

of catalytic activity.

Similar to the Pt/SiO_2 catalyst, the spectrum for the Pt/Al_2O_3 catalyst, at 150°C, is also almost identical to that of the original reactant gas mixtures (noted as 'inlet' in Fig. 4(d)). As temperature is increased to 200°C and 250°C, the NO peak decreases, the C_3H_6 peak disappears, and the N_2O peak experiences a marked increase. Thus, at this temperature, NO gas is partly reduced to N_2O and N_2, and oxygen likely binds to the catalyst (Pt) surface. We observe that NO_2 gas (which indicates an oxidation process on the Pt surface) does not appear at this temperature, though C_3H_6 (which indicates a reduction process on the Pt surface) is no longer available. Thus, the Pt/Al_2O_3 catalyst appears to perform better in NO_x conversion than the Pt/SiO_2 catalyst. Moreover, Pt/Al_2O_3 exhibits clearly higher peak of N_2O gas, suggesting that most of the Pt sites are likely in a reduced state promoting more NO decomposition to N_2 and N_2O. A continuous decrease of N_2O species is observed at 275°C and 300°C while NO_2 concentration is observed to increase to maximum yield of about 26% at these temperatures. In addition, the role of C_3H_6 in consuming the chemisorbed oxygen at the Pt surface over the alumina support becomes insignificant at that temperature, suggesting that the catalyst surface begins to be covered by more chemisorbed atomic oxygen. Finally, in a process similar to that of the Pt/SiO_2 catalyst, as temperature is increased further to 350°C and 400°C, the presence of C_3H_6 and N_2O is minute; suggesting that the oxidation process in Pt is again predominantly arising, which leads to the degradation of catalytic activity. And again, the decrease of NO_2 concentration at such high temperature is affected by the equilibrium concentration (Seker and Gulari, 2000; García-Cortés *et al.*, 2003).

As explained in section 2, the degree of conversion X_R (refer to Eqs. (1)–(2)) for NO and C_3H_6 were measured on the basis of FTIR measurement of gas mixture before and after the gases passed through the catalysts. In addition, the as-obtained conversions of NO to NO_2 and N_2O were used to estimate the conversion of NO to N_2 on the basis of mass balance. Every corresponding conversion of each species was plotted as a function of temperature in Figs. 5(a) and 5(b) for the catalyst of Pt/SiO_2 and Pt/Al_2O_3, respectively. From both figures, C_3H_6 is rapidly consumed almost completely at

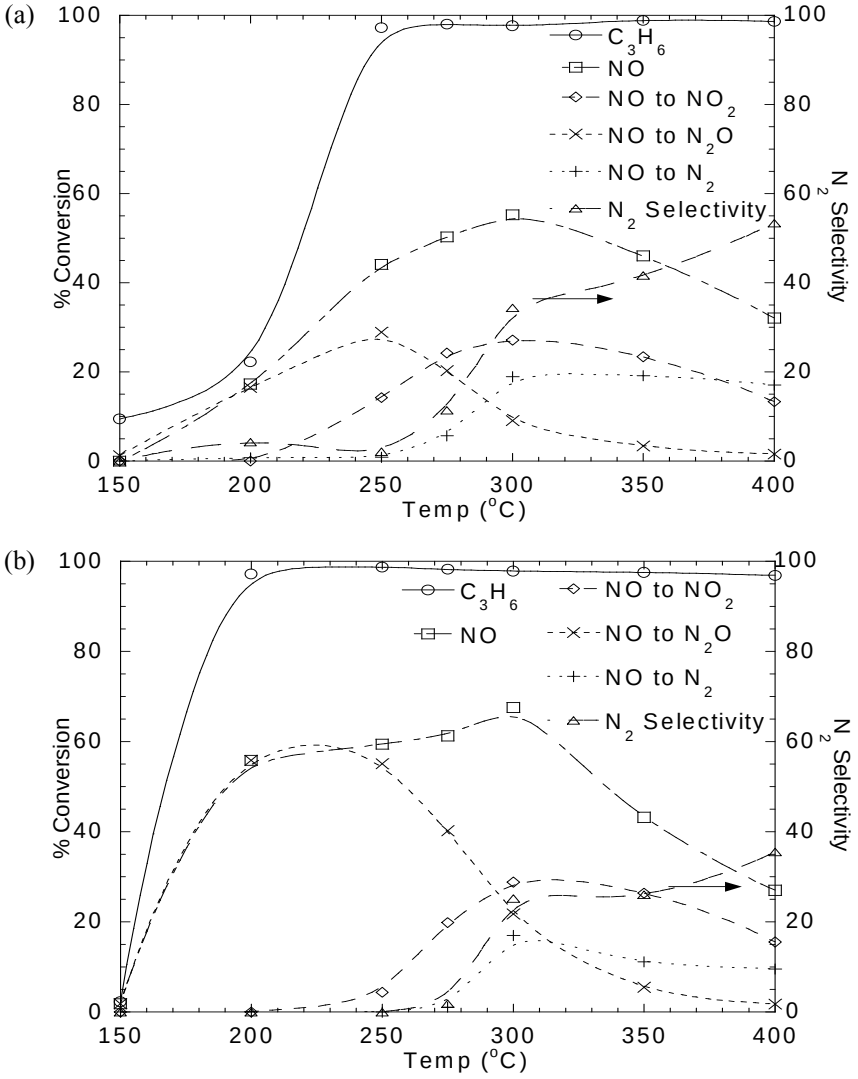

Fig. 5. The NO_x reduction activity of: a) Pt/SiO_2, and b) Pt/Al_2O_3 catalysts.

250°C for Pt/SiO_2 and at 200°C for Pt/Al_2O_3. For NO conversion, the profile exhibits a maximum peak at 55% and 66% conversion at 300°C for Pt/SiO_2 and Pt/Al_2O_3, respectively. However, the higher NO_x conversion of Pt/Al_2O_3 consequently produces more N_2O gas, and therefore reduces the N_2 yield (production) and N_2 selectivity. The maximum conversion of NO to N_2 for both catalysts occurs at 300°C, which corresponds to 20% and 17.5% conversion for Pt/SiO_2 and Pt/Al_2O_3, respectively. As a result, the N_2 selectivity for both catalysts abruptly increases to 50% and 31% for Pt/SiO_2 and Pt/Al_2O_3 at 250°C, respectively. In addition, the maximum yield of NO_2 is produced at the same level for both catalysts, and thus the maximum NO conversions (reduction) to $N_2 + N_2O$ gases for both catalysts reach about 29.8% at 250°C for Pt/SiO_2, and 55.8% at 200~250°C for Pt/Al_2O_3. These facts imply that the catalytic performance of Pt/Al_2O_3 catalyst is likely better than Pt/SiO_2 catalyst in this test.

Before catalytic testing, we performed an extra heat pretreatment in an attempt to further enhance catalytic performance as Després *et al.* (2004) and Kang *et al.* (2005) did. We observe that non-pretreated samples show less NO conversion, 39% and 45% for Pt/SiO_2 and Pt/Al_2O_3 at 250°C, respectively. In order to investigate the effect of the pre-treatment on the Pt catalysts particles, we analyzed pre-treated samples that had been heated up to 700°C under air with a heating rate of 10 °C min^{-1}. The benefit of using air as a carrier gas is that it allows for reducing the PtO monolayer (Després *et al.*, 2004), and increasing the size of Pt particles (García-Cortés *et al.*, 2003; Santiago *et al.*, 2011) to obtain the optimal size for catalytic activity.

Figs. 6(a) and 6(b) show the TEM micrograph of Pt/SiO_2 and Pt/Al_2O_3 particles after heat pretreatment. The size distribution of the pre-treated sample is shown in Fig. 6(c). Here, we recall that Fig. 1(c) shows Pt particles before sintering are homogeneously distributed in a size range of 1.1–3.5 nm, whereas the particles size distribution after sintering is widened to a range of 1–11 nm and 4–11 nm for Pt/SiO_2 and Pt/Al_2O_3, respectively. Pt particles over SiO_2 and Al_2O_3 supports appear less-dispersed than the pristine samples as seen in Figs. 1(a) and 1(b). The mode of size distribution of Pt/SiO_2 is smaller than that of Pt/Al_2O_3, suggesting that there is a stronger interaction between Pt and SiO_2 due to the initial sol-gel reactions within the precursor

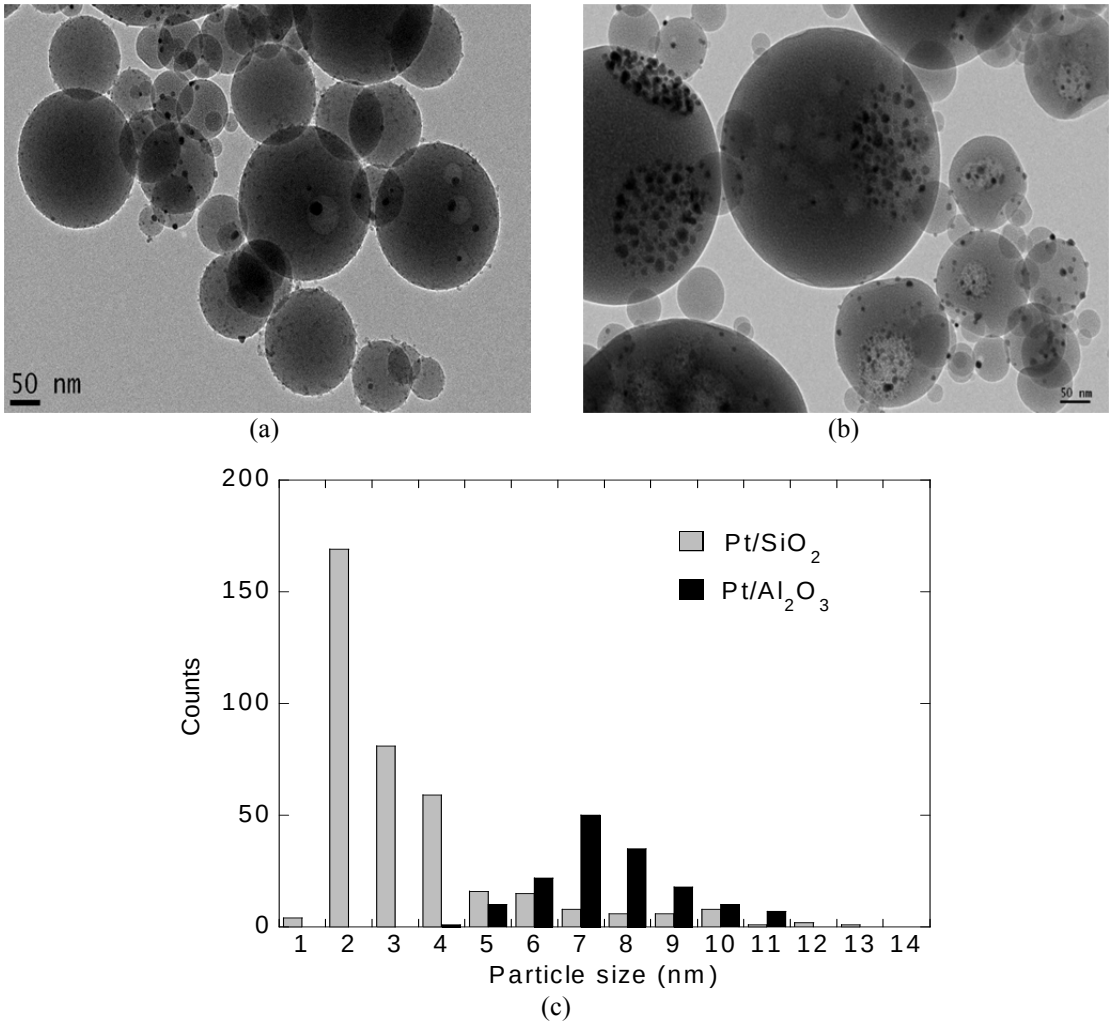

Fig. 6. a) TEM micrograph of the pre-treated sample of Pt/SiO_2, b) TEM micrograph of the pre-treated sample of Pt/Al_2O_3, c) Histogram plot of particle size distribution for the pre-treated samples of Pt/SiO_2 and Pt/Al_2O_3.

solution (see section 2). These reactions thereby reduce the sintering effect, and thus the dispersion of Pt particles over SiO_2 is superior to that of the dispersion of Pt particles over Al_2O_3 after sintering. Well dispersed Pt particles, with sizes larger than 2 nm may show a better NO_x conversion according to previous works (García-Cortés *et al.*, 2003; Vaccaro *et al.*, 2003). In addition, a different Pt particle size may exhibit various reactivity to Pt in which a higher rate of surface reaction may be obtained with large Pt crystallites, as compared to small Pt crystallites (Radic *et al.*, 2004). However, Pt particles that are too large (> 10 nm) are less active due to weaker O bond formation (García-Cortés *et al.*, 2003), while Pt particles that are too small are easily oxidized to PtO which is less active for NOx conversion (García-Cortés *et al.*, 2003). Thus, a moderate size (3–8 nm) of Pt particles is recommended for efficient conversion of NO_x (Jayat *et al.*, 1999; García-Cortés *et al.*, 2003; Vaccaro *et al.*, 2003; Després *et al.*, 2004), therefore, changing the average size of Pt particles over SiO_2 and Al_2O_3 supports from ~2 nm to larger sizes of 3.8 and 8.4 nm may contribute to the NO_x conversion observed in Figs. 5(a) and 5(b).

CONCLUSIONS

Catalyst of well dispersed Pt particles over SiO_2 and Al_2O_3 supports were fabricated successfully via an aerosol method combined with pyrolysis. According to calculations for aerosol particle formation, the solute of Pt particles concentrates locally near the droplet surfaces while TEOS and Al^{3+} diffuse toward the center of the droplets, implying that Pt particles disperse on the metal oxide supports. The results of HR-TEM studies corroborate our calculations showing that the Pt/SiO_2 and Pt/Al_2O_3 catalyst particles were uniformly dispersed at the surface of each supporting material in the respective samples. The XRD patterns confirm that Pt/Al_2O_3 particle size is slightly larger than that of the Pt/SiO_2 particles. The results of XPS and peak deconvolution show that the surface of Pt/SiO_2 and Pt/Al_2O_3 are mostly covered by metallic Pt. Moreover, the maximum NO_x reduction obtained for Pt/SiO_2 and Pt/Al_2O_3 catalysts are 29.8% and 55.8%, at 250°C, respectively.

The Pt particles over SiO_2 and Al_2O_3 supports from pristine catalysts before heat pretreatment are homogeneously distributed with similar particle sizes of ~2 nm. However, the Pt particles sizes are completely different at high temperature after the heat pretreatment, where the sintering effect on Pt over Al_2O_3 is more severe than that of Pt over SiO_2, suggesting that there is a stronger interaction between Pt and the SiO_2 support.

ACKNOWLEDGEMENTS

This work was supported by National Research Foundation of Korea (NRF) grants funded by the Korean Government (MEST) (No. NRF-2010-0019543). It was also supported by the Global Frontier R&D Program of the Center for Multiscale Energy Systems, funded by the National Research Foundation under the Ministry of Education, Science and Technology, Korea (No. 2012M3A6A7054863), and also by the Korea Meteorological Administration Research and Development Program under Grant KMIPA KMIPA2014-21130.

REFERENCES

Asoro, M.A., Kovar, D., Shao-Horn, Y., Allard, L.F. and Ferreira, P.J. (2010). Coalescence and Sintering of Pt Nanoparticles: In Situ Observation by Aberration-corrected HAADF STEM. *Nanotechnology* 21: 025701.

Burch, R. and Millington, P.J. (1995). Selective Reduction of Nitrogen Oxides by Hydrocarbons under Lean-burn Conditions Using Supported Platinum Group Metal Catalysts. *Catal. Today* 26: 185–206.

Burch, R. and Millington, P.J. (1996). Selective Reduction of NO_x by Hydrocarbons in Excess Oxygen by Alumina- and Silica-supported Catalysts. *Catal. Today* 29: 37–42.

Burch, R. and Watling, T.C. (1997). The Effect of Promoters on $Pt/A1_2O_3$ Catalysts for The Reduction of NO by C_3H_6 under Lean-burn Conditions. *Appl. Catal., B* 11: 207–216.

Burch, R. and Watling, T.C. (1998). The Effect of Sulphur on the Reduction of NO by C_3H_6 and C_3H_8 over Pt/Al_2O_3 under Lean-Burn Conditions. *Appl. Catal., B* 17: 131–139.

Burch, R., Sullivan, J.A. and Watling, T.C. (1998). Mechanistic Considerations for the Reduction of NO_x over Pt/Al_2O_3 and Al_2O_3 Catalysts under Lean-burn Conditions. *Catal. Today* 42: 13–23.

Burch, R., Breen, J.P. and Meunier, F.C. (2002). A Review of the Selective Reduction of NO_x with Hydrocarbons under Lean-Burn Conditions with Non-Zeolitic Oxide and Platinum Group Metal Catalysts. *Appl. Catal., B* 39: 283–303.

Burch, R. (2004). Knowledge and Know-How in Emission Control for Mobile Applications. *Catal. Rev. Sci. Eng.* 46: 271–333.

Byeon, J.H. and Kim, J.W. (2014). Fabrication of Bimetallic Nanostructures via Aerosol-Assisted Electroless Silver Deposition for Catalytic CO Conversion. *ACS Appl. Mater. Interfaces* 6: 3105–3110.

Cho, I.H., Park, S.B., Cho, S.J. and Ryoo, R. (1998). Investigation of $Pt/\gamma\text{-}Al_2O_3$ Catalysts Prepared by Sol–Gel Method. *J. Catal.* 173: 295–303.

Choi, I.D., Lee, H., Shim, Y.B. and Lee, D. (2010). A One-Step Continuous Synthesis of Carbon-Supported Pt Catalysts Using a Flame for the Preparation of the Fuel Electrode. *Langmuir* 26: 11212–11216.

Després, J., Elsener, M., Koebel, M., Kröcher, O., Schnyder, B. and Wokaun, A. (2004). Catalytic Oxidation of Nitrogen Monoxide over Pt/SiO_2. *Appl. Catal., B* 50: 73–82.

Dong, T.T.T. and Lee, B.K. (2009). Characteristics, Toxicity, and Source Apportionment of Polycyclic Aromatic Hydrocarbons (PAHs) in Road Dust of Ulsan, Korea. *Chemosphere* 74: 1245–1253.

Firmansyah, D.A., Kim, T., Kim, S., Sullivan, K., Zachariah, M.R. and Lee, D. (2009). Crystalline Phase Reduction of Cuprous Oxide (Cu_2O) Nanoparticles Accompanied by a Morphology Change during Ethanol-Assisted Spray Pyrolysis. *Langmuir* 25: 7063–7071.

Firmansyah, D.A., Kim, S.G., Lee, K.S., Zahaf, R., Kim,

Y.H. and Lee, D. (2012). Microstructure-Controlled Aerosol-Gel Synthesis of ZnO Quantum Dots Dispersed in SiO_2 Nanospheres. *Langmuir* 28: 2890–2896.

García-Cortés, J.M., Pérez-Ramírez, J., Rouzaud, J.N., Vaccaro, A.R., Illán-Gómez, M.J. and Salinas-Martínez de Lecea, C. (2003). On the Structure Sensitivity of DeNOx HC-SCR over Pt-beta Catalysts. *J. Catal.* 218: 111–122.

Gonzalez, R.D., Lopez, T. and Gomez, R. (1997). Sol-Gel Preparation of Supported Metal Catalysts. *Catal. Today* 35: 293–317.

Haj, O.K., Ziyade, S., Ziyad, M. and Garin, F. (2002). DeNOx Reaction Studies Reactivity of Carbonyl or Nitro-compounds Compared to C_3H_6: Influence of Adsorbed Species in N_2 and N_2O Formation. *Appl. Catal., B* 37: 49–62.

Hauff, K., Tuttlies, U., Eigenberger, G. and Nieken, U. (2012). Platinum Oxide Formation and Reduction during NO Oxidation on a Diesel Oxidation Catalyst – Experimental Results. *Appl. Catal., B* 123–124: 107–116.

Hirashima, H., Kojima, C., Kohama, K., Imai, H., Balek, V, Hamada, H. and Inaba, M. (1998). Oxide Aerogel Catalysts. *J. Non-Cryst. Solids* 225:153–156

Hu, L., Boateng, K.A. and Hill, J.M. (2006). Sol–gel Synthesis of Pt/Al_2O_3 Catalysts: Effect of Pt Precursor and Calcination Procedure on Pt Dispersion. *J. Mol. Catal. A: Chem.* 259: 51–60.

Iwamoto, M. (1990). Decomposition of NO on Copper Ion-exchanged Zeolite Catalysts, Proceedings of Meeting on Catalytic Technology for Removal of Nitrogen Monoxide, Tokyo, January 1990, p. 17.

Jayanthi, G.V., Zhang, S.C. and Messing, G.L. (1993). Modeling of Solid Particle Formation during Solution Aerosol Thermolysis: The Evaporation Stage. *Aerosol Sci. Technol.* 19: 478–490.

Jayat, F., Lembacher, C., Schubert, U. and Martens, J.A. (1999). Catalytic NO_x Reduction in Lean Burn Exhaust over Pt/Silica Catalysts with Controlled Pt Particle size. *Appl. Catal., B* 21: 221–226.

Joubert, E., Courtois, X., Marecot, P., Canaff, C. and Duprez, D. (2006). The Chemistry of DeNOx Reactions over Pt/Al_2O_3: The Oxime Route to N_2 or N_2O. *J. Catal.* 243: 252–262.

Kang, M., Bae, Y.S. and Lee, C.H. (2005). Effect of Heat Treatment of Activated Carbon Supports on the Loading and Activity of Pt Catalyst. *Carbon* 43: 1512–1516.

Kim, J.H., Son, M., Sohn, Y. and Shin, W.G. (2013). Hollow SiO_2 Nanospheres: One-Step Synthesis by Introducing Guest Ag Nanoparticles and an Irradiating Electron Beam under Ambient Condition. *Aerosol Air Qual. Res.* 13: 415–420.

Lee, J.H., Beaucage, G. and Pratsinis, S.E. (1997). Aero-Sol-Gel Synthesis of Nanostructured Silica Powders. *Chem. Mater.* 9: 2400–2403.

Lee, S.G., Choi, S.M. and Lee, D. (2007). The Role of Salt in Nanoparticle Generation by Salt-Assisted Aerosol Method: Microstructural Changes. *Thermochim. Acta* 455: 138–147.

Lenggoro, I.W., Hata, T., Iskandar, F., Lunden, M.M. and Okuyama, K. (2000). An Experimental and Modeling Investigation of Particle Production by Spray Pyrolysis Using a Laminar Flow Aerosol Reactor. *J. Mater. Res.* 15: 733–743.

Li, L. and Guan, N. (2009). HC-SCR Reaction Pathways on Ion-exchanged ZSM-5 Catalysts. *Microporous Mesoporous Mater.* 117: 450–457.

Lin, L.Y., Wang, C.Y. and Bai, H. (2015). A Comparative Investigation on the Low-temperature Catalytic Oxidation of Acetone over Porous Aluminosilicate-supported Cerium Oxides. *Chem. Eng. J.* 264: 835–844.

Lu, H., Amagai, T. and Ohura, T. (2011). Comparison of Polycyclic Aromatic Hydrocarbon Pollution in Chinese and Japanese Residential Air. *J. Environ. Sci.* 23: 1512–1517.

Männikkö, M., Skoglundh, M. and Ingelsten, H.H. (2012). Selective Catalytic Reduction of NO_x with Methanol over Supported Silver Catalysts. *Appl. Catal., B* 119–120: 256–266.

Mulla, S.S., Chena, N., Cumaranatunge, L., Blau, G.E., Zemlyanov, D.Y., Delgass, W.N., Epling, W.S. and Ribeiro, F.H. (2006). Reaction of NO and O_2 to NO_2 on Pt: Kinetics and Catalyst Deactivation. *J. Catal.* 241: 389–399.

Nagai, Y., Hirabayashi, T., Dohmae, K., Takagi, N., Minami, T., Shinjoh, H. and Matsumoto, S. (2006). Sintering Inhibition Mechanism of Platinum Supported on Ceria-based Oxide and Pt-oxide–support Interaction. *J. Catal.* 242: 103–109.

Pitchon, V. and Fritz, A. (1999). The Relation between Surface State and Reactivity in the DeNOx Mechanism on Platinum-Based Catalysts. *J. Catal.* 186: 64–74.

Pornpan, N. and Paisan, K. (2015). Synthesis of Copper-Based Nanostructured Catalysts on SiO_2–Al_2O_3, SiO_2–TiO_2, and SiO_2–ZrO_2 Supports for NO Reduction. *J. Nanosci. Nanotechnol.* 15: 5410–5417.

Radic, N., Grbic, B. and Terlecki-Baricevic, A. (2004). Kinetics of Deep Oxidation of n-hexane and Toluene over Pt/Al_2O_3 Catalysts Platinum Crystallite Size Effect. *Appl. Catal., B* 50: 153–159.

Reid, R.C., Prausnitz, J.M. and Poling, B.E. (1987). *The Properties of Gases and Liquids*, 4th ed., McGraw-Hill, New York.

Romero-Pascual E., Larrea, A., Monzon, A. and Gonzalez, R.D. (2002). Thermal Stability of Pt/Al_2O_3 Catalysts Prepared by Sol-Gel. *J. Solid State Chem.* 168: 343–353.

Roy, S., Hegde, M.S. and Madras, G. (2009). Catalysis for NO_x Abatement. *Appl. Energy* 86: 2283–2297.

Santiago, M., Restuccia A., Grammb, F. and Pérez-Ramírez, J. (2011). Spray Deposition Method for the Synthesis of Supported Catalysts with Superior Metal Dispersion. *Microporous Mesoporous Mater.* 146: 6–81.

Seker, E. and Gulari, E. (2000). Activity and N_2 Selectivity of Sol–Gel Prepared Pt/Alumina Catalysts for Selective NO_x Reduction. *J. Catal.* 194: 4–13.

Smith, D.M., Welch, W.F., Graham, S.M., Chughtai, R., Wicke, B.G. and Grady, K.A. (1998). Reaction of Nitrogen Oxides with Black Carbon: An FT-IR Study. *Appl. Spectrosc.* 42: 674–680.

Sobczak, I., Kusior, A. and Ziolek, M. (2008). FTIR Study

of NO, C_3H_6 and O_2 Adsorption and Interaction on Gold Modified MCM-41 Materials. *Catal. Today* 137: 203–208.

Strobel, R., Stark, W.J., Mädler, L., Pratsinis, S.E. and Baiker, A. (2003). Aerosol Flame Synthesis of Catalysts. *J. Catal.* 213: 296–304.

Strobel, R., Baiker, A. and Pratsinis, S.E. (2006). Flame-made Platinum/Alumina: Structural Properties and Catalytic Behaviour in Enantioselective Hydrogenation. *Adv. Powder Technol.* 17: 457–480.

Suzuki, A., Nakamura, K., Sato, R., Okushi, K., Tsuboi, H., Hatakeyama, N., Endou, A., Takaba, H.; Kubo, M., Williams, M.C. and Miyamoto, A. (2009). Multi-scale Theoretical Study of Support Effect on Sintering Dynamics of Pt. *Surf. Sci.* 603: 3049–3056.

The European parliament and the Council of The European Union (2007). Regulation (EC) No 715/2007 of the European Parliament and of the Council of 20 June 2007 on Type Approval of Motor Vehicles with Respect to Emissions from Light Passenger and Commercial Vehicles (Euro 5 and Euro 6) and on Access to Vehicle Repair and Maintenance Information, L 171, Official Journal of the European Union, pp. 1–16.

Thirupathi, B., Rajesh, K. and Smirniotis, P.G. (2012). Low-temperature Selective Catalytic Reduction of NO with NH_3 over V/ZrO_2 Prepared by Flame-assisted Spray Pyrolysis: Structural and Catalytic Properties. *Appl. Catal., B* 127: 255–264.

Tshilongo, J., Botha, A., Rensburg, M.J.V., Leshabane, N. and Ntsasa, N.G. (2009). FTIR and GC as Complementary Tools for Analysis of Corrosive Gases. *Accred. Qual.* 14: 655–663.

Vaccaro, A.R., Mul, G., Pérez-Ramırez, J. and Moulijn, J.A. (2003). On the Activation of Pt/Al_2O_3 Catalysts in HC-SCR by Sintering: Determination of Eedox-active Sites Using Multitrack. *Appl. Catal., B* 46: 687–702.

Wang, L., Xing, D.M., Liu, Y.H., Cai, Y.H., Shao, Z.G., Zhai, Y.F., Zhonga, H.X., Yi, B.L. and Zhang, H.M. (2006). Pt/SiO_2 Catalyst as an Addition to Nafion/PTFE Self-humidifying Composite Membrane. *J. Power Sources* 161: 61–67.

Wang, L., Huang, B., Su, Y., Zhou, G., Wanga, K., Luo, H. and Ye, D. (2012). Manganese Oxides Supported on Multi-walled Carbon Nanotubes for Selective Catalytic Reduction of NO with NH_3: Catalytic Activity and Characterization. *Chem. Eng. J.* 192: 232–241.

Wang, T., Yang, S., Sun, K. and Fang, X. (2011). Preparation of Pt/beta Zeolite–Al_2O_3/Cordierite Monolith for Automobile Exhaust Purification. *Ceram. Int.* 37: 621–626.

Yoon, S., Panov, A.G., Tonkyn, R.G., Ebeling, A.C., Barlow, S.E. and Balmer, M.L. (2002). An Examination of the Role of Plasma Treatment for Lean NO_x Reduction over Sodium Zeolite y and gamma alumina. Part 1: Plasma Assisted NO_x Reduction Over NAy and Al_2O_3. *Catal. Today* 72: 243–250.

Zhang, R., Shi, D., Zhao, Y., Chen, B., Xue, J., Liang, X. and Lei, Z. (2011). The Reaction of $NO+C_3H_6+O_2$ Over the Mesoporous SBA-15 Supported Transition Metal Catalysts. *Catal. Today* 175: 26–33.

Received for review, April 10, 2015
Revised, June 15, 2015
Accepted, August 19, 2015